RSC Advances

PAPER

View Article Online
View Journal | View Issue

Cite this: *RSC Adv.*, 2017, **7**, 41527

Ni(II) and Co(II) complexes of an asymmetrical aroylhydrazone: synthesis, molecular structures, DNA binding, protein interaction, radical scavenging and cytotoxic activity†

Yueqin Li, *[a] Zhiwei Yang,[a] Minya Zhou,[a] Yun Li,[a] Jing He,[a] Xuehong Wang[a] and Zhengfeng Lin[b]

Two new nickel(II) and cobalt(II) benzhydrazone complexes having the general formula [$ML_2phen\cdot 3CH_3OH$] (where M = Ni and Co, L = 2-acetonaphthonebenzoylhydrazone, phen = 1,10-phenanthroline) have been synthesized *via* the reaction of $Ni(OAc)_2\cdot 4H_2O$ and $CoCl_2\cdot 6H_2O$ with 2 equivalents of HL and 1 equivalent of phen ligands in a MeOH/THF mixed medium. Both complexes have been characterized by single-crystal X-ray crystallography methods, which reveals a distorted octahedral coordination environment around the metal center with an MN_4O_2 chromophore [M = Ni(II) and Co(II)], with the hydrazone ligand acting as a monoanionic bidentate N,O-donor. These complexes exhibit quasi-reversible one-electron reduction responses (Ni^{II}–Ni^{I}, Co^{II}–Co^{I}) within the $E_{1/2}$ at −0.808 and −0.767 V *versus* Ag/AgCl reference. The DNA-binding interactions of the complexes with herring sperm DNA have been investigated by UV-vis absorption, emission and viscosity measurements, which reveal that the complexes could interact with DNA *via* intercalation. The protein binding interactions of the complexes with BSA were investigated by UV-vis, fluorescence and synchronous fluorescence methods, which indicate strong binding of the complexes with BSA and a static quenching mechanism was observed. The Ni(II) complex displays higher DNA and BSA-binding affinity than the corresponding Co(II) analogue, which is expected of its smaller size. Moreover, the potential for free-radical scavenging of all the complexes was also determined using DPPH, hydroxyl and nitric oxide radicals under *in vitro* conditions, showing that the complexes are more effective in arresting the formation of hydroxyl than nitric oxide or DPPH radicals. Cytotoxicity experiments reveal that the two complexes both exhibit cytotoxic effects against human hepatocellular carcinoma cell line SMMC-7721 and human lung adenocarcinoma cell line A549.

Received 16th May 2017
Accepted 14th August 2017

DOI: 10.1039/c7ra05504h

rsc.li/rsc-advances

Introduction

Cancer is one of the most fatal non-communicable diseases which causes a significant number of deaths every year. Chemotherapy is currently the most-utilized treatment for cancer treatment. *cis*-Platin and platinum drugs are some of the most widely used cytotoxic chemotherapeutic agents.[1,2] Although they are active in the treatment of several types of cancer, the dose-limiting nephrotoxicity and the development of drug resistance prevent their potential efficacy.[1–3] Therefore, in efforts to improve the efficacy and overcome the side effects, numerous transition metal complexes have been synthesized and tested for their anticancer activities.[4,5] Several ruthenium-, gold-, gallium-, titanium-, and arsenic-based compounds have been investigated for their anticancer potential;[6–11] however, none of these compounds have been approved clinically. It should be noted that reviews devoted to the general use of nickel and cobalt complexes in medicine have been published.[12,13] A large body of evidence indicates that nickel and cobalt chelates are an effective method to inhibit tumor growth, and they have become promising agents in the treatment of cancer.[14–25]

The effect of metal-based pharmaceuticals depends not only on the function of the metal but also on ligand moieties.[26] Schiff base derivatives of hydrazones are an important class of ligands with interesting ligation properties due to the presence of several coordination sites. Moreover, the hydrazone unit offers a number of interesting features such as a degree of rigidity, a conjugated π-system and a NH unit that readily participates in hydrogen bonding and may be a site of protonation–deprotonation. It has been proved that hydrazone derivatives play

[a]*School of Chemical Engineering, Nanjing Forestry University, Nanjing 210037, P. R. China. E-mail: yueqinli@163.com; Fax: +86-025-85427024; Tel: +86-025-85427024*

[b]*Inspection and Quarantine Technology Centre, Hainan Entry-exit Inspection and Quarantine Bureau, Haikou 570311, P. R. China*

† Electronic supplementary information (ESI) available: FTIR, ESI-mass and cyclic voltammograms of the complexes. CCDC 1511152 and 1518021. For ESI and crystallographic data in CIF or other electronic format see DOI: 10.1039/c7ra05504h

vital role in certain pharmaceutical functions such as DNA binding and cleavage,[18] antibacterial,[27] and anticancer.[28] In addition, the use of heterocyclic diimine as the co-ligand in ternary complexes is of considerable interest because some of the diimine containing nickel and cobalt complexes exhibit interesting biological as well as pharmacological properties.[29] The pivotal role of diimine ligands in antitumour activities have been clarified by numerous literatures earlier.[30,31] Overall, it has been demonstrated that physicochemical features, such as planarity, hydrophobicity, and size of the diimine, the nature of the co-ligand, and the coordination geometry of the metal complex, all played important roles in determining the binding mode of transition metal complexes to DNA.

DNA is the primary intracellular target of anti-cancer drugs, the interaction between small molecules and DNA can cause DNA damage in cancer cells, hence blocking the division of cancer cells and resulting in cell death. A study on the interaction of small molecules with DNA on a molecular level is very important in the development of novel chemotherapeutics and highly sensitive diagnostic agents.[32,33] Small molecules can interact with DNA through the following three non-covalent modes: intercalation, groove binding and external static electronic effects.[34] Both the planarity of ligand and the coordination geometry of the metal ion play important roles in deciding the intercalating ability of complexes to DNA.[35,36] It has been proved that increasing the size of the substituent and planarity of ligands can enhance the DNA interaction and protein binding.[17,37,38] Therefore, planar aromatic groups, such as benzyl and napthyl group were introduced as substituent to enhance planarity of the ligand. By varying the metal center, it is possible to modify the mode as well as the extent of interaction of the complex with nucleic acids and facilitate individual applications. On the other hand, serum albumins play an important and efficient role in drug delivery due to their remarkable binding properties. With the advantages of low cost and ready availability, bovine serum albumin (BSA) is a widely used serum albumin. The interaction of drug–protein may react in the formation of a stable protein complex which has important effect on the distribution, absorption, metabolism and properties of drugs. Such an interactions of drug compounds have aromatic rings are very important for protein sterilization and different regulation processes.[39] Therefore, the activity of metal complexes towards DNA and protein BSA is useful in the design and synthesis of metal-based anticancer therapeutics.

Based on the above facts, we have been intense in studying the role of presence of aromatic rings, planarity and molecular composition of nickel and cobalt complexes on DNA and protein binding and cytotoxicity. Hence, our present investigation focuses on the synthesis of two new nickel and cobalt complexes containing 2-acetonaphthone benzoyl hydrazone ligand (HL) and 1,10-phenanthroline (phen) co-ligand. The structure of the new complexes has been characterized by various spectro-analytical and crystallographic techniques. All the synthesized compounds have been subjected to different experiments to assess their interacting ability with DNA/protien and antioxidant and cytotoxicity potential.

Experimental

Materials and instrumentation

2-Acetonaphthone benzoyl hydrazone (HL) has been synthesized and its molecular structure has been obtained previously by our group.[40] 1,10-Phenanthroline monohydrate, ethidium bromide (EB), herring sperm DNA, tris(hydroxymethyl) aminomethane hydrochloride (Tri–HCl), bovine serum albumin (BSA), 2,2-diphenyl-1-picrylhydrazyl (DPPH), *cis*-platin were purchased from Sigma-Aldrich Chemicals and used as received. Human hepatocellular carcinoma cell SMMC-7721 and human lung adenocarcinoma cell A549 were purchased from Shanghai Cell Bank, Chinese Academy of Sciences. SRB, fetal bovine serum and all other cell-culture reagents were obtained from Solarbio Science and Technology Co., Ltd. Beijing, China. All other chemicals and reagents used for biological studies were of high-quality biological grade.

Elemental analyses for C, H and N were performed on a Perkin Elmer 240C elemental analyzer. ESI-MS spectra for the complexes were collected on a Thermo Fisher LTQ Orbitrap XL Electrospray Ionization Mass Spectrometer in a positive ion mode. FT-IR measurements (KBr pellets) were recorded in the range of 400–4000 cm^{-1} on the instrument of Thermo Nicolet Nexus 670 infrared spectrometer. Ultraviolet-visible (UV-vis) spectroscopy was obtained on a Varian Cary 300 UV-vis spectrophotometer. Fluorescence spectroscopy was measured with Perkin Elmer LS-55 spectrometer at room temperature.

Synthesis of $NiL_2phen \cdot 3CH_3OH$ (1)

HL (0.576 g, 2 mmol) was dissolved in 10 mL MeOH/THF (V/V = 1 : 1) solution, to which 2 mmol of triethylamine (0.201 g) was added. A solution of nickel acetate tetrahydrate (0.176 g, 1 mmol) in MeOH (10.0 mL) was added dropwise to the ligand solution, which was stirred at room temperature. After 1 h, a methanolic solution of 1,10-phenanthroline monohydrate (0.180 g, 1 mmol) was slowly added to the reaction mixture, resulting in a yellow green colour solution. The reaction mixture was allowed to stir for another 2 h, after which the precipitate that formed was filtered, washed successively with 2 mL of MeOH and 10 mL diethyl ether, and then dried at room temperature. X-ray quality single crystals, having a green colour and prime shape appeared on slow evaporation of the filtrate at room temperature. Yield 0.309 g (34%). Anal. calc for $C_{53}H_{50}N_6O_5Ni$ (909.70 g mol^{-1}): C 69.79, H 5.54, N 9.23%; found: C 69.70, H 5.57, N 9.31%. FTIR (KBr, cm^{-1}): 1589 and 1523 s $\upsilon_{(C=N-N=C)}$, 1369 s $\upsilon_{(C-O)}$. ESI-MS (MeOH): m/z = 813.25 $[NiL_2Phen + H]^+$ (calculated m/z = 812.24 for NiL_2Phen^+).

Synthesis of $CoL_2phen \cdot 3CH_3OH$ (2)

2-Acetonaphthone benzoyl hydrazone (0.576 g, 2 mmol) was dissolved in 10 mL MeOH/THF (V/V = 1 : 1) solution, to which 2 mmol of triethylamine (0.201 g) was added. A solution of cobalt chloride hexahydrate (0.129 g, 1 mmol) in MeOH (10.0 mL) was added dropwise to the ligand solution, which was stirred at room temperature. After one hour a methanolic solution of 1,10-phenanthroline monohydrate (0.180 g, 1 mmol)

was slowly added to the reaction mixture, resulting in a deep brown colour solution. The reaction mixture was allowed to stir for another 2 h, after which the precipitate that formed was filtered, washed successively with 2 mL of MeOH and 10 mL diethyl ether, and then dried at room temperature. X-ray quality single crystals, having a brown colour and square shape appeared on slow evaporation of the filtrate at room temperature. Yield 0.529 g (58%). Anal. calc for $C_{53}H_{50}N_6O_5Co$ (909.92 g mol^{-1}): C 69.96, H 5.53, N 9.23%; found: C 69.90, H 5.57, N 9.31%. FTIR (KBr, cm^{-1}): 1589 and 1517 s $\upsilon_{(C=N-N=C)}$, 1367 s $\upsilon_{(C-O)}$. ESI-MS (MeOH): m/z 846.24 $[CoL_2Phen\cdot CH_3OH + H]^+$, (calculated m/z = 845.26 for $[CoL_2Phen\cdot CH_3OH]^+$).

X-ray crystallography

The X-ray single-crystal data for complex **1** and **2** were recorded on a Brucker SMART Apex CCD detector diffractometer with graphite-monochromated MoKα radiation ($\lambda = 0.71073$ Å). The collected data were reduced using the SAINT program,[41] and multi-scan absorption corrections were performed using the SADABS program.[42] The structures were solved by direct methods and refined by full-matrix least squares on F^2 using SHELXL-97.[43] All non-hydrogen atoms were refined anisotropically and the hydrogen atoms in these structures were located *via* the difference Fourier map and constrained to ideal positions in the refinement procedure. Experimental details for X-ray data collection complexes are presented in Table 1.

Table 1 Crystallographic data and structure refinement parameter of complexes

Compound	**1**	**2**
Formula	$C_{53}H_{50}N_6O_5Ni$	$C_{53}H_{50}N_6O_5Co$
FW	909.70	909.92
Crystal system	Monoclinic	Monoclinic
Space group	$P2_1/c$	$P2_1/c$
a (Å)	10.334(2)	10.360(6)
b (Å)	15.835(3)	15.843(9)
c (Å)	28.718(6)	28.627(15)
α (°)	90	90
β (°)	103.504(6)	103.660 (18)
γ (°)	90	90
V (Å^3)	4569.5(16)	4566(4)
Z	4	4
D_{calc} (g cm^{-3})	1.322	1.324
μ (mm^{-1})	0.48	0.43
F (000)	1912	1908
Crystal size	0.30 × 0.25 × 0.15	0.23 × 0.20 × 0.18
Theta range (°)	2.6–26.5	2.4–20.3
Limiting indices	$-10 \le h \le 12$	$-11 \le h \le 12$
	$-15 \le k \le 18$	$-18 \le k \le 18$
	$-34 \le l \le 33$	$-33 \le l \le 33$
Reflections collected	23 095	30 500
Independent reflections	8089	7997
Data/restraints/ parameters	8089/0/594	7997/0/591
T (K)	296	293
Goodness of fit on F^2	1.05	0.97
Final R indices$[I > 2\sigma(I)]$	$R_1 = 0.0384$,	$R_1 = 0.0726$,
	w$R_2 = 0.1094$	w$R_2 = 0.1862$
R indices (all data)	$R_1 = 0.0597$,	$R_1 = 0.1513$,
	w$R_2 = 0.1281$	w$R_2 = 0.2539$
R_{int}	0.029	0.102
ρ_{max}, ρ_{min} (e Å^{-3})	0.36, −0.51	1.09, −1.35

Cyclic voltammetry

Cyclic voltammogram (CV) was recorded on a CHI 660C electrochemical work station using a three-electrode cell in which a platinum plate, a saturated Ag/AgCl and a platinum foil are used as the working, reference and auxiliary electrodes, respectively. A ferrocene/ferrocenium (Fc/Fc^+) couple was used as an internal standard. Cyclic voltammograms of the complexes were recorded in DMF solutions at a scan rate of 100 mV s^{-1}. Tetra-*n*-butylammonium perchlorate (TBAP, 0.1 M) was used as the supporting electrolytes. Prior to every electrochemical assay, the solutions were deoxygenated by purging them with nitrogen. All electrochemical measurements were performed at room temperature.

DNA binding studies

Experiments involving the binding of compounds to herring sperm DNA were performed in double-distilled water with 5 mM Tris–HCl and 50 mM NaCl solution and the pH was adjusted to 7.2 with hydrochloric acid. DNA solution was prepared with 50 mM NaCl solution. The UV absorbance ratio at 260 and 280 nm (A_{260}/A_{280}) of 1.85 indicated that the DNA was sufficiently free of protein contamination.[44] The concentrations of DNA were determined spectrophotometrically by assuming $\varepsilon_{260} = 6600\ M^{-1}\ cm^{-1}$,[45] which was found to be 3.72×10^{-4} mol L^{-1} when the mass concentration was 200 μg mL^{-1}. The ligand and complexes were dissolved in a combined solvent of 5% DMSO and 95% Tris–HCl buffer for all experiments. A stock solution of DNA was stored at 4 °C and used after no more than 4 days.

UV-vis titration experiments were performed by keeping a fixed concentration of the metal complex constant (25 μM) and varying the nucleotide concentration (0–125 μM). However, when obtaining the absorption spectra, equal amounts of DNA were added to both complex and reference solutions to eliminate the absorbance of DNA itself. The complex-DNA solutions were allowed to incubate for 30 min before the absorption spectra were recorded.

Further support for the binding of complexes to DNA *via* intercalation was obtained using fluorescence spectral techniques in order to point out whether a complex can displace EB from a DNA–EB complex. EB displacement experiments were carried out by adding solutions of the complexes to a Tris–HCl buffer solution (pH 7.2) of a DNA/EB mixture. DNA was pretreated with EB at a [DNA]/[EB] ratio of 10 for 30 min at room temperature, then a test solution was added to this mixture of EB–DNA and the change in fluorescence intensity was measured. The excitation wavelength was fixed at 545 nm for EB bound to DNA. Emissions were recorded with increasing concentrations of compounds and the emission range was adjusted before measurements. The ligand and complexes (0–50 mM) were then added to the mixture and their effect on the emission intensity was measured.

Viscosity experiments were carried on an Ubbelohde viscometer of 10 mL capacity, immersed in a thermostated water bath maintained at 37.0 ± 0.1 °C. The stock solutions of DNA (50 μM) and complexes (0–50 μM) were prepared in Tris–HCl/NaCl buffer. Mixing of the solutions was achieved by purging the nitrogen gas through viscometer. The flow time was measured three times for each sample with a digital stopwatch, and the mean flow time was calculated. Data were presented as $(\eta/\eta_0)^{1/3}$ *versus* binding ratio [complex]/[DNA], where η and η_0 are the specific viscosity of DNA in the presence and absence of complex, respectively. The values of η and η_0 were calculated from the relation:[46] $\eta_0 = (t - t_b)/t_b$, where t_b is the flow time of buffer alone, and t is the observed flow time for DNA in the presence of complex. Relative viscosities for DNA were obtained from the relation, η/η_0.

Protein binding studies

The protein-binding interactions of the ligand and complexes with BSA were investigated using both of fluorescence spectra and UV-vis absorption. Fluorescence spectra were obtained with an excitation wavelength of 280 nm and an emission wavelength of 345 nm corresponding to those of free BSA. The excitation and emission slit widths and scan rates were maintained at a constant for all experiments. Samples were thoroughly degassed using pure nitrogen gas for 15 minutes using quartz cells (4 × 1 × 1 cm) with high-vacuum Teflon stopcocks. Stock solutions of BSA were prepared in 50 mM phosphate buffer (pH 7.2) and stored in the dark at 4 °C for additional use. Concentrated stock solutions of metal complexes were prepared by dissolving them in DMSO : Tris–HCl buffer (5 : 95) and diluted suitably with phosphate buffer to obtain appropriate concentrations. 2.5 mL of BSA solution (1 μM) was titrated by successive additions of a 5 μL stock solution of complexes (10^{-4} M) using a micropipette. Synchronous fluorescence spectra were also obtained using the same concentrations of BSA and complexes as mentioned above with two different values of $\Delta\lambda$ (difference between the excitation and emission wavelengths of BSA) such as 15 and 60 nm. For UV-vis absorption experiment, a 3 mL solution of BSA (1 μM) was titrated with various concentrations of the complexes. Equal solutions of complexes were added to the reference solutions to eliminate the absorbance of the complexes themselves. The UV-vis absorption spectra were measured from 200 to 400 nm.

Antioxidant activity

The DPPH (2,2-diphenyl-1-picrylhydrazyl) radical-scavenging activity of the compounds was measured according to the method described by Blois.[47] The DPPH radical is a stable free radical having a λ_{max} of 517 nm. Various concentrations (10–60 μM) of the test compounds were added to a solution of DPPH (125 mM, 2 mL) in methanol and the final volume was made up to 4 mL with double-distilled water. The solution was incubated at 37 °C for 30 min in the dark. The decrease in the absorbance of DPPH was measured at 517 nm. The same experiment carried out without the test compounds served as a control.

The hydroxyl radical (OH˙) in aqueous media was generated by the Fenton system.[48] The solution of the tested complex was prepared with DMF. The 5 mL assay mixture contained following reagents: safranin (20 μM), EDTA–Fe^{2+} (200 μM), H_2O_2 (196 mM), the tested compounds (1–6 μM) and a phosphate buffer (40 μM, pH = 7.4). The assay mixtures were incubated at 30 °C for 10 min in a water bath. The sample without the tested compound was used as the control. After that, the absorbance was measured at 520 nm.

Nitric oxide (NO) radical-scavenging activity was determined based on the reported method, in which sodium nitroprusside in an aqueous solution at physiological pH spontaneously generates nitric oxide, which interacts with oxygen to produce nitrate ions that can be estimated using the Griess reagent.[49] For the experiment, sodium nitroprusside (10 mM) in phosphate buffered saline was mixed with a fixed concentration of the compound and incubated at room temperature for 150 min. After the incubation period, 0.5 mL of the Griess reagent containing 1% sulfanilamide, 2% H_3PO_4 and 0.1% *N*-(1-naphthyl) ethylenediamine dihydrochloride was added. The reaction mixture without the sample but with equivalent amount of solvent served as a control. The absorbance of the chromophore formed was measured at 546 nm.

In the case of the above three assays, all of the tests were run in triplicate. All data are expressed as mean ± standard deviation (SD). Various concentrations of the compounds were used to fix a concentration at which the compounds showed in and around 50% of activity. The percentage of activity was calculated using the formula, % of activity = $[(A_0 - A_C)/A_0] \times 100$. A_0 and A_C are the absorbance in the absence and presence of the tested compounds respectively. The 50% activity (IC_{50}) can be calculated using the percentage of activity results.

In vitro cytotoxic activity evaluation by SRB assays

In vitro cytotoxic activities of the two complexes and *cis*-platin were evaluated against two cancer cell lines including SMMC-7721 and A549 by using the Sulforhodamine B (SRB) assay. All cells were cultured in RPMI 1640 supplemented with 10% (v/v) fetal bovine serum, 1% (w/v) penicillin (10^4 U mL^{-1}) and 10 mg mL^{-1} streptomycin. Cell lines are maintained at 310 K in a 5% (v/v) CO_2 atmosphere with 95% (v/v) humidity. Cultures were passaged weekly using trypsin–EDTA to detach the cells from their culture flasks. The two complexes and cisplatin were dissolved in DMSO and diluted to the required concentration with culture medium when used. The content of DMSO in the final concentrations did not exceed 0.1%. At this concentration, DMSO was found to be non-toxic to the cells tested. Rapidly growing cells were harvested, counted, and incubated at the appropriate concentration in 96-well micro plates for 24 h. The two complexes and cisplatin dissolved in culture medium were then applied to the culture wells to achieve final concentrations ranging from 10^{-4} to 10^2 μM. Control wells were prepared by addition of culture medium without cells. The plates were incubated at 37 °C in a 5% CO_2 atmosphere for 48 h. Upon completion of the incubation, the cells were fixed with icecold 10% trichloroacetic acid (100 mL) for 1 h at 277 K, washed five

times in distilled water and allowed to dry in the air and stained with 0.4% SRB in 1% acetic acid (100 mL) for 15 min. The cells were washed four times in 1% acetic acid and air-dried. The stain was solubilized in 10 mM unbuffered tris base (100 mL) and the OD of each well was measured at 540 nm on a microplate spectrophotometer. The IC_{50} values were calculated from the curves constructed by plotting cell survival (%) *vs.* the complexes concentration (μM). The medium without samples served as a control and triplicate measurements were made for all concentrations. All data are expressed as mean ± SD.

Results and discussion

Benzhydrazone ligand derivative, as a pale yellow crystalline solid, were prepared in high yield by the condensation of 2-acetonaphthone with benzoylhydrazine in an equimolar ratio.[40] It was then reacted with $Ni(OAc)_2 \cdot 4H_2O$ and $CoCl_2 \cdot 6H_2O$ in a 1 : 2 molar ratio, respectively, followed by 1,10-phen in the presence of triethylamine in a 2 : 1 : 1 : 2 molar proportion in methanol at room temperature (Scheme 1). After a few days, single crystals were obtained from the reaction mixture on slow evaporation at room temperature. The elemental analyses data, ESI-MS and FTIR of the complexes are consistent with their formulation as bis-hydrazone complexes of Ni(II) and Co(II) containing phen an ancillary ligand. The synthesized complexes were sparingly soluble in solvents such as ethanol, methanol or acetonitrile and readily soluble only in solvents such as DMF and DMSO, producing intensely orange-colored solutions.

The infrared spectra of the ligand and complexes **1** and **2** were showed in Fig. S1 (ESI†). The free ligand displayed a medium to strong band at 3348 cm^{-1}, which is characteristic of the N–H functional group. The free ligands also displayed $\upsilon_{C=O}$ absorption at 1666 cm^{-1} and $\upsilon_{C=N}$ absorption at 1519 cm^{-1}, which indicate that the ligands exist in the amide form in the solid state. However, bands that are due to υ_{N-H} and $\upsilon_{C=O}$ stretching vibrations were not observed with the complexes, which indicates that the ligands underwent tautomerization and subsequent coordination of the imidolate enolate form during complexation. Coordination of the ligand to the Ni(II) and Co(II) ion through an azomethine nitrogen is expected to reduce the electron density in the azomethine link and thus lower the absorption frequency after complexation (1517–1589 cm^{-1}), which indicates the coordination of azomethine nitrogen to the metal ions. The presence of a new band at 487 cm^{-1}, which is due to υ(Ni–O) and υ(Co–O), is another indication of the involvement of the oxygen of the enolate group in coordination.[50] The appearance of new additional bands in the regions 817 cm^{-1} and 711 cm^{-1} are due to phen ring Ar–H and C=N stretching vibrations respectively.[29]

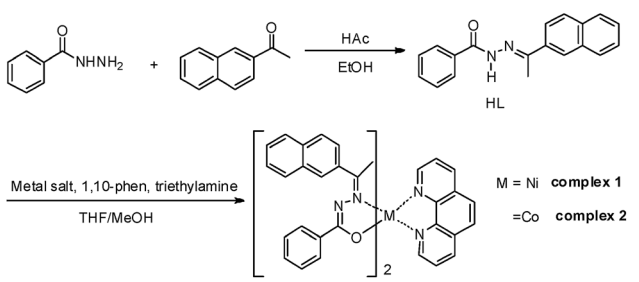

Scheme 1 Synthesis of the ligand and complexes **1** and **2**.

The UV-vis absorption spectra of the ligand and complexes **1** and **2** were obtained in methanol solution (10 μM) in the range of 200–800 nm at room temperature, as presented in Fig. 1. The spectrum of the hydrazone ligand displayed three absorption bands at 234, 278 and 306 nm. Generally, the bands appearing in the 230–280 nm range can be due to the π–π* transition within the aromatic rings, and the band at 306 nm can be due to the n–π* transitions within the >C=N–N chromophore.[15] In the case of the complexes, the bands appeared at 232, 270 and 303 nm. The slight shift in the absorption bands indicated the formation of the metal complexes and the fact that the azomethine nitrogen is involved in coordination.[15,51] The band at 303 nm become broader in complexes than that in the HL, the reason could be assigned to ligand to metal (ion) charge transfer (LMCT) transitions.[51] Unfortunately the expected weak d–d transition in the visible region for the one-electron paramagnetic complexes cannot be detected even with concentrated solutions. It may be lost in the low energy tail of the charge transfer transition.

Single-crystal X-ray crystallography

All the synthesized compounds were analyzed by single crystals X-ray diffraction to confirm the molecular structures and geometry. The crystal structures of nickel and cobalt complexes are shown in Fig. 2 and slected bond distances (Å) and bond angles (°) are given in Table 2. The bond lengths and bond angles of HL can be found in our previous report.[40] Both complexes are crystallized in the monoclinic space group $P2_1/c$ with four molecules in the unit cell. The hexacoordinated Ni(II) and Co(II) center in **1** and **2** respectively, adopt a distorted octahedral geometry with NiN_4O_2 and CoN_4O_2 chromophores, the metal atom being coordinated by two N atoms and two O atoms of the two bidentate Schiff base ligands, along with two N

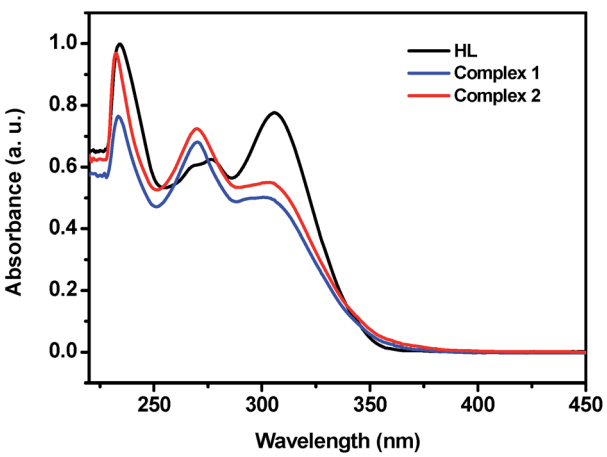

Fig. 1 UV-vis absorption spectra of the ligand, and complexes **1** and **2** in MeOH solution.

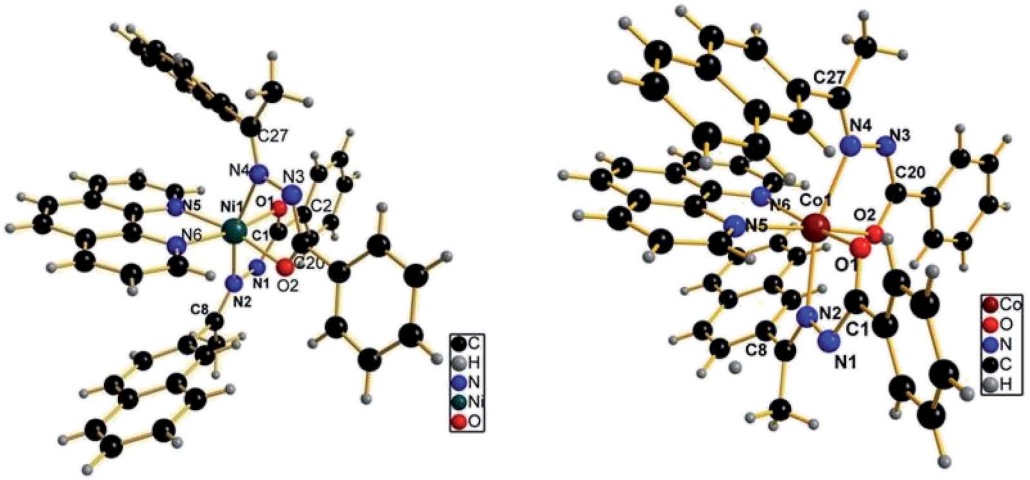

Fig. 2 The coordination environment of Ni(II) and Co(II) complexes.

Table 2 Selected bond lengths (Å) and bond angles (°)

$C_{53}H_{50}N_6O_5Ni$ (1)		$C_{53}H_{50}N_6O_5Co$ (2)	
Bond lengths (Å)	Bond angles (°)	Bond lengths (Å)	Bond angles (°)
N1–N2 1.418(2)	O1–Ni1–N2 77.00(6)	N1–N2 1.412(5)	O1–Co1–N2 76.90(13)
N3–N4 1.417(2)	O1–Ni1–N4 89.62(6)	N3–N4 1.393(6)	O1–Co1–N4 92.95(13)
N1–C1 1.134(3)	O1–Ni1–N5 95.82(7)	N1–C1 1.131(6)	O1–Co1–N5 92.82(17)
N2–C8 1.282(3)	O1–Ni1–N6 170.73(7)	N2–C8 1.287(6)	O1–Co1–N6 164.32(17)
O1–C1 1.271(3)	O1–Ni1–O2 93.90(7)	O1–C1 1.264(6)	O1–Co1–O2 97.13(17)
C1–C2 1.495(3)	O2–Ni1–N2 91.40(6)	C1–C2 1.505(6)	O2–Co1–N2 91.32(16)
Ni1–N2 2.170(2)	O2–Ni1–N4 77.88(6)	Co1–N2 2.205(4)	O2–Co1–N4 75.63(16)
Ni–N4 2.1611(19)	O2–Ni1–N5 168.07(7)	Co1–N4 2.219(4)	O2–Co1–N5 168.22(14)
Ni1–N5 2.1247(19)	O2–Ni1–N6 93.30(7)	Co1–N5 2.193(5)	O2–Co1–N6 96.44(18)
Ni1–N6 2.123(2)	N2–Ni1–N4 162.33(7)	Co1–N6 2.178(4)	N2–Co1–N4 162.49(17)
Ni1–O1 2.0020(16)	N5–Ni1–N2 84.09(7)	Co1–O1 2.019(3)	N5–Co1–N2 84.79(17)
Ni1–O2 2.0076(16)	N5–Ni1–N4 109.03(7)	Co1–O2 2.007(4)	N5–Co1–N4 110.24(17)
	N6–Ni1–N2 108.67(7)		N6–Co1–N2 110.61(15)
	N6–Ni1–N4 86.18(6)		N6–Co1–N4 82.84(15)
	N6–Ni1–N5 77.81(8)		N6–Co1–N5 74.69(18)

atoms of phen. In complex **1**, each of the two bidentate hydrazone ligands coordinates through imine nitrogen and enolate oxygen atoms. The two nitrogen atoms from the two hydrazone ligands are *trans* to each other and the corresponding enolate oxygen atoms are *cis* to each other. Each of the N atoms of phen is *trans* to an enolate oxygen atom. The bond lengths in the Ni(II) complex are: N1–N2 = 1.418(2) (L), N1–C1 = 1.314(3) (S), N2–C8 = 1.282(3) (S), O1–C1 = 1.271(3) (L), C1–C2 = 1.495 (S) Å, (L = longer, S = shorter) (Table 2), which are longer or shorter than those of the corresponding distances in the free ligand[40] due to the bonding of the Ni(II) centre with the ligand. The Ni–O bond lengths (2.0020(16) and 2.0076(16) Å) are in the range of those expected for the Ni(II) ion in an octahedral environment.[29] The Ni–N distances range from 2.123(2) to 2.170(2) Å, with the Ni–N(phen) distances being about 0.03 Å shorter than the Ni–N(imine) distances. In octahedral Ni(II) complexes of aroylhydrazones, it is generally found that the Ni–O bond distance is longer than the Ni–N distance. However, in the present case a reverse trend is observed. In fact, the Ni–N distance in this complex is comparatively longer than that normally observed for octahedral Ni(II) complexes of aroylhydrazones,[28,52] but it is very similar to that reported for an anthracene aldehyde Schiff base complex of Ni(II),[29] and the steric bulk of the naphthalene moiety may be responsible for this relatively longer Ni–N bond. The N6–Ni1–N5 angle (bite angle of phen) is 77.81(8)°, whereas for the hydrazone ligand, the bite angles lie in the range 77.00(6) to 77.88(6)°. The distortion, from a regular octahedral geometry is evident from the N2–Ni1–N4 *trans*-bond angle value of 162.33(7)°, while the other two *trans* angles, O1–Ni1–N6 and O2–Ni1–N5 are 170.73(7) and 168.07(7)°, respectively, which are closer to that expected for an octahedral geometry.

In complex **2**, the Co(II) ion is also in a distorted octahedral environment, having a *cis*-, *trans*-, *cis*-arrangement of the O2, N2 (hydrazone), N2 donor atoms, with each hydrazone ligand acting as a monoanionic bidentate donor, coordinating through the azomethine N, deprotonated amide O atoms and bidentate

N,N-donor of phen ligand. The Co–N distances range from 2.178(4) to 2.205(4) Å. Like the previously described Ni(II) complex, in the Co(II) complex, the Co–N(phen) distances are also about 0.03 Å shorter than the Co–N(imine) distances. The bond distances for Co–O1 and Co–O2 are 2.019(3) and 2.007(4) Å, respectively, which are comparable to the bond lengths reported for octahedral Co(II) complexes of aroylhydrazone.[16] The bite angle of phen (N5–Co1–N6 angle) is 74.69(18)°, whereas for the hydrazone ligand, the bite angles vary between 75.63(16) and 76.70(13)°. The distortion, from a regular octahedral geometry is evident from the N2–Co1–N4 *trans*-bond angle value of 162.49(17)°, while the other two *trans* angles, O1–Co1–N6 and O2–Co1–N5 are 164.32(17) and 168.22(14)°, respectively. When compared the corresponding bond lengths of the Ni(II) complex with that of the Co(II) complex, it was found that the distances of Ni–N and Ni–O are both shorter than the corresponding Co–N and Co–O bond distances. In addition, and the bite angles of the Co(II) complex were more deviate from the ideal bond angles of 90° and 180° than that of the Ni(II) complex, which indicate that Co(II) complex has a more distorted octahedral geometry. X-ray determination confirms the structure that was proposed on the basis of spectroscopic data, which is consistent with the bivalency of the metal and the monoionic nature of the ligand in the complexes.

Electrochemical studies

Electrochemical studies were carried out for Ni(II) and Co(II) benzhydrazone complexes in DMF solution under an atmosphere of nitrogen. Tetrabutylammonium perchlorate (TBAP) (0.05 M) was used as the supporting electrolyte and the concentration of the complexes was 500 μM. The cyclic voltammograms of complexes are shown in Fig. S4 and Fig. S5 (ESI†), respectively. Both complexes were redox active and exhibit quasi reversible redox wave assignable to M^{2+}/M^{+} couple. For complex **1**, the cathodic and anodic peak potential was −0.935 and −0.681 V, respectively. While for complex **2**, the corresponding value was −0.788 and −0.747 V, respectively. The separation of the cathodic and anodic peak potential, ΔE_p was 0.254 and 0.041 V for **1** and **2**, respectively. The formal potential $E^{0\prime}$ (or voltammetric $E_{1/2}$), taken as the average of E_{pc} and E_{pa} was −0.808 and −0.767 V for **1** and **2**, respectively. Between −1.5 to −2.0 V, reductive waves are observed, which correspond to reductions of the phen ligand.[29] The single-electron nature of the voltammograms was confirmed by a comparison of the current heights for the complexes and that for a simple $[NiL_2]$ complex (where L = thiophene aldehyde benzhydrazone) under identical conditions.[15] The redox potentials were virtually independent of the scan rates, which indicates quasi-reversibility.[53] In general, the reason for quasi-reversible electron transfer in the above complexes may either be due to slow electron transfer or the deposition of the complex on the electrode surface.

DNA-binding studies

DNA is the primary pharmacological target of many antitumor compounds. DNA–metal complex interactions are of paramount importance in understanding the mechanism of tumour inhibition in the treatment of cancer. The interaction of the ligand HL and complexes **1** and **2** with DNA was studied by a number of techniques, such as absorption spectral titration, fluorescence spectroscopy and viscosity measurements.

UV-vis absorption studies. Electronic absorption spectroscopy is commonly employed to determine the binding ability of metal complexes with a DNA helix. Complexes bound to DNA through intercalation often show a decrease in molar absorptivity (hypochromism) and a red shift (bathochromism) of their electronic absorption bands due to the strong stacking interaction between the aromatic chromophores of the complex and base pairs of DNA.[54] The extent of shift and hypochromism are commonly found to correlate with the intercalative binding strength. The absorption spectrum of HL and its Ni(II) and Co(II) complexes in the absence and presence of herring sperm DNA are shown in Fig. 3. Upon incremental additions of DNA to the test compounds, the following changes were observed. In the presence of DNA, the absorption bands of HL exhibited hypochromism of about 40.30% at 306 nm. However, complexes **1** and **2** exhibited the hypochromism of about 59.73% and 58.29% at 231 nm, 50.03% and 52.38% at 269 nm, respectively, accompanied by bathochromic shifts of 2–3 nm, which shows that both Ni(II) and Co(II) benzhydrazone complexes were bound strongly to DNA *via* the intercalative mode. The observed hypochromism was due to stacking interactions between the aromatic chromophores of the complexes and DNA base pairs, which is consistent with the intercalative mode of binding.[15,20,55] These observations are similar to those were reported earlier for various metallointercalators.[55,56]

In order to compare quantitatively the binding strength of the compounds, the intrinsic binding constants (K_b) of them with CT-DNA were determined from the following eqn (1):[57]

$$[DNA]/(\varepsilon_a - \varepsilon_f) = [DNA]/(\varepsilon_b - \varepsilon_f) + 1/K_b(\varepsilon_b - \varepsilon_f) \quad (1)$$

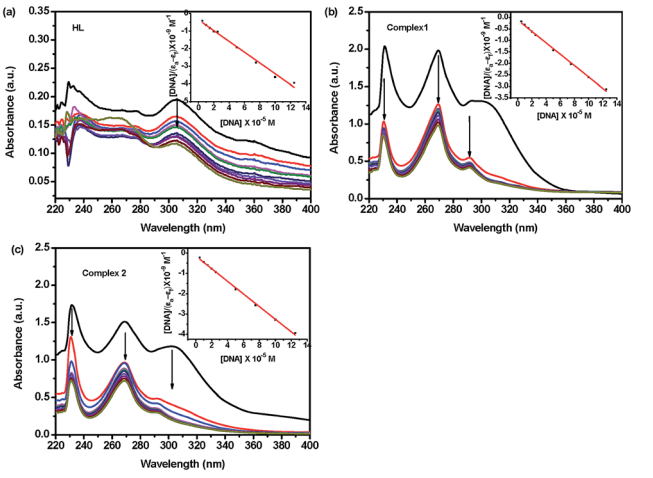

Fig. 3 Electronic absorption spectra of HL (a) and complex **1** (b) and complex **2** (c) (25 μM) with increasing concentrations of DNA (0, 5, 10, 15, 20, 25, 50, 75, 100, 125 μM). Arrows show the changes in absorbance with respect to an increase in the DNA concentration (insert plots of [DNA] *versus* $[DNA]/(\varepsilon_a - \varepsilon_f)$).

where [DNA] is the concentration of DNA in base pairs, the apparent extinction coefficient ε_a is obtained by calculating A_{obs}/[complex], ε_f corresponds to the extinction coefficient of the complex in its free form and ε_b refers to the extinction coefficient of the complex in the fully bound form. Each set of data, fitted to the above equation, gave a straight line with a slope of $1/(\varepsilon_b - \varepsilon_f)$ and y-intercept of $1/K_b(\varepsilon_b - \varepsilon_f)$. The K_b value was determined from the ratio of the slope to intercept,[57] which were found to be $8.12(\pm0.05) \times 10^4\ M^{-1}$, $2.19(\pm0.12) \times 10^5\ M^{-1}$ and $2.08(\pm0.09) \times 10^5\ M^{-1}$, corresponding to HL, **1** and **2**, respectively. The magnitude of the binding constant value clearly showed that complex **1** bound more strongly with DNA than the ligand and complex **2** through an intercalative mode.

Competitive binding between EB and complexes for DNA. Generally, steady-state competitive binding experiments using metal complexes as quenchers provide some information about the binding of the complexes to DNA. Ethidium bromide (EB) is a planar cationic dye that is widely used as a sensitive fluorescence probe for native DNA. EB emits intense fluorescent light in the presence of DNA due to its strong intercalation between the adjacent DNA base pairs. This displacement technique is based on the decrease of fluorescence intensity resulting from the displacement of bound EB from a DNA sequence by a quencher and the quenching is due to the reduction of the number of binding sites on the DNA that is available to the EB. Hence, this method serves as indirect evidence to identify intercalative binding modes. In our study, changes in the intensity as well as the position of the emission band of EB bound DNA were monitored after the addition of metal complex solution. The above said emission band in the spectra of combined nickel hydrazone complex–DNA system showed a significant bathochromic shift with a simultaneous reduction in the fluorescence intensity (35.89%, 76.96% and 82.61%, respectively) revealing that the EB molecules are displaced from their DNA binding sites by the added complexes. The fluorescence spectrum of EB bound-DNA quenched by the ligand and complexes is shown in Fig. 4 with the Stern–Volmer plot as an inset to the figures. The observed linearity in the plot supported the fact that the quenching of EB bound to DNA by the test complex is in good agreement with the linear Stern–Volmer eqn (2):

$$I_0/I = 1 + K_q[Q] \quad (2)$$

where I_0 is the emission intensity in the absence of quencher, I is the emission intensity in the presence of quencher, K_q is the quenching constant, and [Q] is quencher concentration. The K_q value is obtained as a slope from the plot of I_0/I *versus* [Q]. The quenching plots illustrate that the quenching of EB bound to DNA by free ligands and complexes are in good agreement with the linear Stern–Volmer equation. In the Stern–Volmer plots of I_0/I *versus* [Q], the quenching constant (K_q) is given by the ratio of the slope to intercept. The K_q value obtained for the ligand and complexes **1** and **2** were found to be $5.71(\pm0.13) \times 10^3\ M^{-1}$, $5.04(\pm0.20) \times 10^4\ M^{-1}$ and $3.46(\pm0.14) \times 10^4\ M^{-1}$, respectively. Further, the binding constant (K_{app}) value obtained for the ligand and complexes **1** and **2** using the following equation:

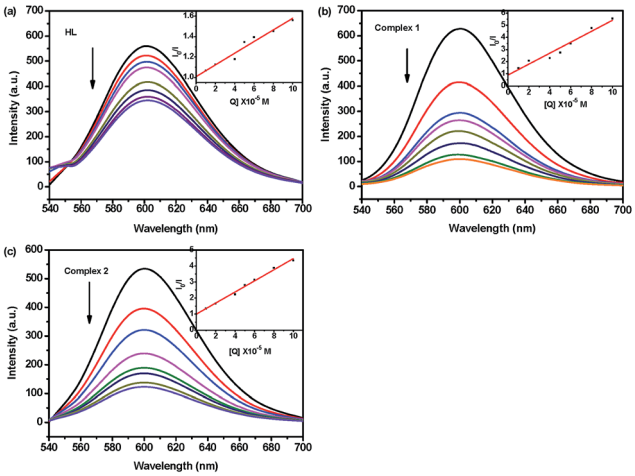

Fig. 4 Emission spectra of DNA–EB (50 μM), in the presence of 0, 10, 20, 40, 50, 60, 80 and 100 μM of compounds. The arrow indicates the changes in the emission intensity as a function of complex concentration (inset: Stern–Volmer plot of the fluorescence titration data).

$K_{EB}[EB] = K_{app}[compound]$. Where the compound concentration has the value at a 50% reduction of the fluorescence intensity of [EB], $K_{EB} = 1.0 \times 10^7\ M^{-1}$, and [EB] = 2.5 μM, were $4.37 \times 10^3\ M^{-1}$, $1.0 \times 10^6\ M^{-1}$, and $8.53 \times 10^5\ M^{-1}$, respectively. These data suggested that the interaction of the Ni(II) and Co(II) complexes with DNA is stronger than that of the free ligand, which is consistent with the absorption spectral observations. Since these changes indicated only one kind of quenching process, it may be concluded that all the compounds bind to DNA *via* the same mode. Furthermore, such quenching constants and binding constants of the ligands and complexes suggest that the interaction of all the compounds with DNA should be of intercalation.[55,58] On the basis of all the spectroscopic studies, we concluded that the free hydrazone ligand and complexes can bind to DNA *via* an intercalative mode and that the complexes **1** and **2** bind to DNA more strongly than the free ligand.

Viscosity studies. Though optical photophysical methods are employed to monitor the binding mode of the metal complex with the DNA, hydrodynamic measurements are preferred as the confirmation tests. Viscosity measurements are sensitive to changes in the length of DNA molecule and regarded as least ambiguous and most critical test for the binding mode. EB as a classical intercalator shows a significant increase in relative viscosity of the DNA solution on intercalation due to an increase in overall DNA contour length on binding to DNA.[46] In contrast, partial or non-classical intercalation of complex would bend or kink the DNA helix, shortening the effective length of the DNA, and reducing DNA viscosity accordingly, while the electrostatic and groove binding cause little or no effect on the relative viscosity of DNA solution.[59] In order to clarify the binding mode and strength of complexes with DNA, the DNA viscosity variance at room temperature was studied by varying the concentration of complexes. The values of relative viscosity $(\eta/\eta_0)^{1/3}$ were determined and plotted against the values of [DNA]/[complex]. The effect of EB, HL and complexes **1** and **2** on the viscosity

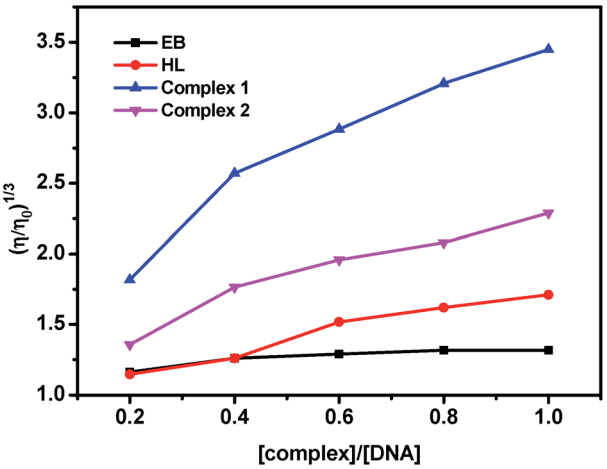

Fig. 5 Effect of increasing amounts of EB, HL and complex **1** and **2** on the relative viscosity of DNA at 37.0 ± 0.1 °C. [DNA] = 50 μM and [compound] = 0–50 μM.

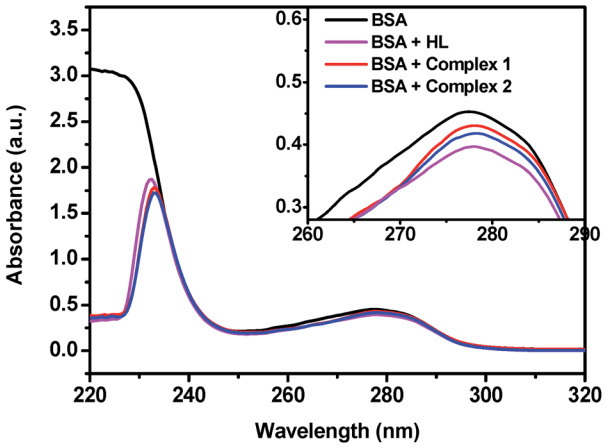

Fig. 6 Absorption spectra of BSA (10 μM) in the present of the ligand and complexes **1** and **2** (10 μM).

of rod-like DNA is shown in Fig. 5. The relative viscosity of DNA exhibits a considerable increase in the presence of increasing amounts of the complexes. Such behaviour indicates that the complexes are inserted between the DNA bases, thus resulting in an intercalative mode of binding between DNA and each complex. The binding ability of complexes to increase the viscosity of DNA follows the order 1 > 2 > HL. The increase in viscosity of DNA by complexes suggests insertion of aromatic ring into the base pairs of DNA as discussed above. Complex **1** showed a greatest effect on viscosity of DNA among all the compounds and higher than of EB, indicating the nature of the central metal is also effective in increasing the length of DNA biopolymer.[60] Thus, all these observations suggest that both complexes can bind to DNA through intercalation. The observed viscosity results were in accordance with absorption titration results.

Protein binding studies

Absorption spectral studies. UV-vis absorption spectroscopy is a common method to explore the structural changes of proteins and investigate protein complex formation.[61] The absorption spectrum of BSA shows two bands, a strong band in the range of 220–240 nm related to the absorption of the protein backbone (α-helix structure) and a weak one around 278 nm due to the absorption of aromatic amino acids (Trp, Tyr, and Phe).[62,63] It is well known that the absorption maximum of BSA is highly sensitive to the surrounding microenvironment and displays a substantial spectral shift upon changes in the protein conformation.[64] The UV-visible spectral measurement can also distinguish the type of quenching *i.e.*, static or dynamic quenching. Dynamic quenching only affects the excited states of the fluorophores and hence there are no changes in the absorption spectra. However, ground-state complex formation will frequently result in perturbation of the absorption spectrum of the fluorophore.[51] Fig. 6 indicates that the BSA skeleton absorption intensity in the range of 220–240 nm decreases upon adding the compound because of perturbation of the secondary structure of the protein.[63,65] Subtle changes in the maximum absorption at 278 nm were also observed, which indicate a perturbation of the α-helix induced by a specific interaction between the complexes and BSA.[66] There was a small blue shift of about 2 nm for all the complexes but not for the ligand. These phenomena revealed the existence of a static interaction between BSA and the added complexes due to the formation of the ground state complex of the type BSA-complex reported earlier.[17,66,67]

Fluorescence quenching of BSA by HL and complexes. It is well known that the transport of drugs through the bloodstream is affected by the interaction of drugs with blood plasma proteins, in particular serum albumin. Analysis of the binding of chemical compounds to BSA has been commonly undertaken by examining fluorescence spectra. The binding of BSA to compounds was studied by fluorescence measurements at room temperature. Various concentrations of the ligand and complexes **1** and **2** were added to solutions of BSA (1 μM) and fluorescence spectra were obtained in the range of 290–450 nm upon excitation at 280 nm. The effects of the compounds on the fluorescence emission spectrum of BSA are given in Fig. 7. Upon addition of the ligand and complexes to a solution of BSA at an emission wavelength of 345 nm, decreases of emission intensity up to 27.47%, 72.78% and 60.36% from the initial fluorescence intensity of BSA accompanied by a hypsochromic shift of 1–2 nm for all compounds were observed, respectively. The blue shift that was observed was mainly due to the fact that the active site of the protein is buried in hydrophobic environment. These results suggest strong interaction of all compounds with BSA protein.[25,37]

Binding analysis. To investigate the quenching process further, fluorescence quenching data were analyzed with the Stern–Volmer equation and Scatchard equation.[16] The quenching constant (K_q) can be calculated using the plots I_0/I *versus* [Q] (shown in Fig. 7) and was found to be $3.67(\pm0.13) \times 10^4$ M^{-1}, $2.73(\pm0.10) \times 10^5$ M^{-1} and $1.54(\pm0.04) \times 10^5$ M^{-1}, corresponding to the HL and complexes **1** and **2**. The binding

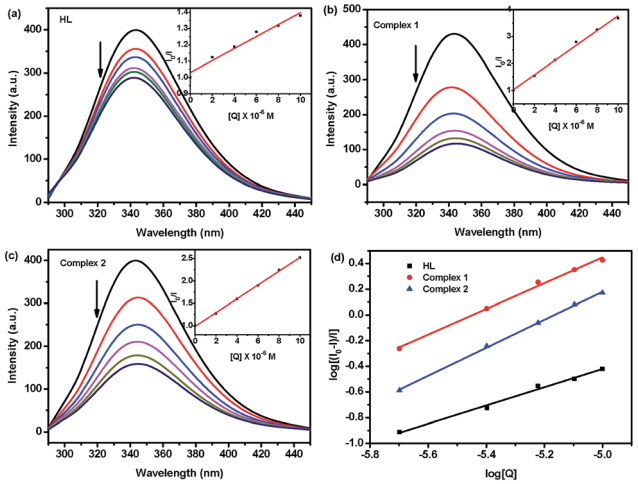

Fig. 7 (a–c) Emission spectra of BSA (1 μM; λ_{ex} = 280 nm; λ_{em} = 345 nm) as a function of concentration of the compounds (0, 2, 4, 6, 8 and 10 μM). Arrow indicates the effect of the compound on the fluorescence emission of BSA (inset: plot of [Q] *vs.* I_0/I). (d) Scatchard plots of the fluorescence titration of the ligand and the complexes with BSA.

constant of the compounds on binding with BSA can be calculated using the Scatchard eqn (3):

$$\log[(I_0 - I)/I] = \log K_{bin} + n \log[Q] \quad (3)$$

where K_{bin} is the binding constant of compound with DNA and n is the number of binding sites. From the plot of $\log[(I_0 - I)/I]$ *versus* log[Q] (Fig. 7d), the number of binding sites (n) and the binding constant (K_{bin}) have been obtained. The calculated K_{bin} and n values are given in Table 3. The calculated value of n is around one for all the compounds indicating the existence of a single binding site in BSA for the ligand and the complexes. The values of K_q and K_{bin} for the ligand and complexes suggested that the complexes interact with BSA more strongly than the ligand. These calculated values of K_q and K_{bin} for all of the complexes suggested that the complexes interact more strongly with BSA than DNA. The Ni(II) complexes show both DNA and BSA binding affinities higher than the analogous Co(II) complexes, which is expected of the smaller size of Ni(II) complex [Ni1–N2, 2.170(2); Ni–N4, 2.1611(19); Ni1–N5, 2.1247(19); Ni1–N6, 2.123(2); Ni1–O1, 2.0020(16); Ni1–O2, 2.0076(16) Å] to fit well into the DNA/BSA grooves than the bulkier cation of Co(II) complex [Co1–N2, 2.205(4); Co1–N4, 2.219(4); Co1–N5, 2.193(5); Co1–N6, 2.178(4); Co1–O1, 2.019(3); Co1–O2; 2.007(4) Å]. The binding ability is also in line with the natural order of stability. So, it is clear that the sizes of the metal complexes make a major contribution in determining the DNA/BSA binding affinities of 3d metal complexes.[38]

Table 3 The quenching constant (K_q), binding constant (K_{bin}) and number of binding sites (n) for the interactions of the compounds with BSA

Compound	K_q (M^{-1})	K_{bin} (M^{-1})	n
HL	$3.67(\pm0.13) \times 10^4$	$1.35(\pm0.06) \times 10^3$	0.71(±0.04)
Complex **1**	$2.73(\pm0.10) \times 10^5$	$4.30(\pm0.15) \times 10^5$	0.95(±0.05)
Complex **2**	$1.54(\pm0.04) \times 10^5$	$1.49(\pm0.11) \times 10^5$	1.09(±0.07)

Characteristics of the synchronous fluorescence spectra. To investigate the structural changes that occurred in BSA upon the addition of our compounds, synchronous fluorescence spectra of BSA were measured before and after the addition of test compounds to get valuable information on the molecular microenvironment, particularly in the vicinity of the fluorophore functional groups.[68] According to Miller,[69] in synchronous fluorescence spectroscopy the difference between the excitation and emission wavelengths ($\Delta\lambda = \lambda_{em} - \lambda_{ex}$) reflects the spectra of a different nature of chromophores. If the $\Delta\lambda$ value is 15 nm, the synchronous fluorescence of BSA is characteristic of a tyrosine residue, whereas a larger $\Delta\lambda$ value of 60 nm is characteristic of tryptophan.[70] The synchronous fluorescence spectra of BSA with various concentrations of test compounds were recorded at $\Delta\lambda$ = 15 nm and $\Delta\lambda$ = 60 nm and are shown in Fig. 8. In the synchronous spectra of BSA at $\Delta\lambda$ = 15 nm, it became clear that an increase in the concentration of the ligand added to BSA increased (very slightly) the intensity of the synchronous fluorescence spectral band corresponding to the tyrosine residue. However, complexes **1** and **2** showed an obvious decrease in the fluorescence intensity of the same band at 287 nm, up to 57.17% and 51.62% of the initial fluorescence intensity of BSA, along with a bathochromic shift of 1 nm. This shows that complexes **1** and **2** affected tyrosine

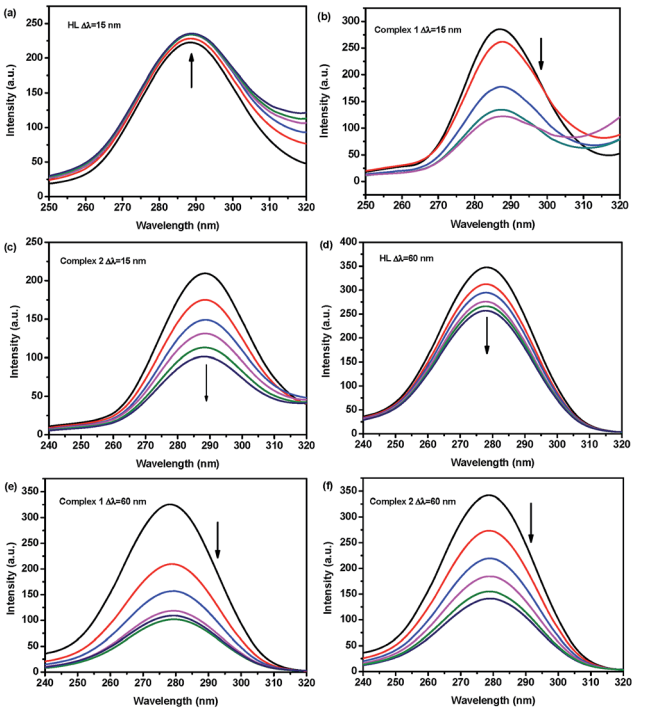

Fig. 8 The synchronous spectra of BSA (1 μM) in the presence of increasing amounts of the ligand and complexes (0, 2, 4, 6, 8 and 10 μM) at a wavelength difference of $\Delta\lambda$ = 15 nm and $\Delta\lambda$ = 60 nm. The arrow shows the emission intensity changes upon an increase in the concentration of the compounds.

residues whereas the ligand did not affect the environment in the above said region. At the same time, in the case of the synchronous fluorescence spectra of BSA at $\Delta\lambda = 60$ nm, the addition of the compounds to the solution of BSA resulted in significant decrease in the fluorescence intensity of BSA at 278 nm, up to 26.00%, 68.68% and 58.73% of the initial fluorescence intensity of BSA accompanied with a blue shift of 1–2 nm for the ligand and the complexes, respectively. These results indicated that the ligand affected only the tryptophan residue but not tyrosine residue, whereas complexes **1** and **2** affected both the micro environments *i.e.*, tyrosine and tryptophan residues, the effect was more towards tryptophan residues than tyrosine residue. The features of synchronous measurements confirmed that conformational changes occurred in BSA upon interaction with the complexes. Similar behaviour regarding the interaction between the BSA and metal hydrazone complexes was reported earlier.[18,37,51] The hydrophobicity observed in fluorescence and synchronous measurements confirmed the effective binding of all the complexes with BSA. Hence, the strong interaction of these new nickel(II) octahedral complexes with BSA suggested that the complexes may be suitable for anticancer studies.

Antioxidant activities

Since the experiments conducted so far revealed that Ni(II) and Co(II) complexes exhibit good DNA and protein binding affinity, it is considered worthwhile to study the antioxidant activity of these compounds. Many Ni(II) and Co(II) complexes bearing hydrazone ligands are known to have radical scavenging properties.[15,16,71] The radical scavenging activities of our compounds in a cell free system have been examined with reference to hydroxyl radical ($OH^{\bullet}$), DPPH radical ($DPPH^{\bullet}$) and nitric oxide ($NO^{\bullet}$) radical and their corresponding IC_{50} values have been tabulated in Table 4. The inhibitory effect of the hydrazone ligand and complexes on radicals was also depicted in Fig. 9, showing the suppression ratio increases with increasing concentration in the range of tested concentration. The order of the suppression ratio for $DPPH^{\bullet}$ and $OH^{\bullet}$ is complex **1** > complex **2**, while for the NO radicals, the scavenging ability is very close to each other. Even though the $DPPH^{\bullet}$ scavenging ability of complexes were lower than the standards, such as butylated hydroxyanisole (BHA) and butylated hydroxytoluene (BHT) studied in references,[16] the ability was excellent for the DPPH and OH radicals when compared to the standards radicals (Table 4). The IC_{50} values (Table 4) indicated that the various radical scavenging activities of the complexes are in the order of $OH^{\bullet} > DPPH^{\bullet} > NO^{\bullet}$. It is to be noted that no significant radical scavenging activities were observed in all the experiments carried out with $Ni(OAc)_2 \cdot 4H_2O$ and $CoCl_2 \cdot 6H_2O$, even up to 1.0 mmol of concentration under the same experimental conditions. It can be concluded that the scavenging effects of the free ligand is significantly less when compared to that of its corresponding Ni(II) and Co(II) complexes, which is mainly due to the chelation of the organic ligand with the Ni(II) and Co(II) ions. Although the IC_{50} values observed in NO scavenging assay show much lower NO scavenging ability than those of the reported nickel(II) benzhydrazone complexes[15,25] and cobalt(II) hydrazone complexes,[25,30] the IC_{50} values observed in DPPH and HO scavenging assay do demonstrate that both complexes have a comparable effective in arresting the formation DPPH radicals as well as an obvious stronger OH scavenging potential. Therefore, the complexes have significant potential to be applied as scavengers to eliminate the DPPH and HO radicals.

Table 4 The radical scavenging activity of the complexes and standards BHA and BHT

	IC_{50} values (μM)		
Compound	$DPPH^{\bullet}$	$HO^{\bullet}$	$NO^{\bullet}$
HL	>60	>6	>500
Complex **1**	35.0 ± 2.0	3.1 ± 0.1	452 ± 7
Complex **2**	55.0 ± 3.2	5.7 ± 0.1	438 ± 9
BHA[a]	10.2 ± 0.8	274 ± 9	623 ± 12
BHT[a]	9.92 ± 0.63	312 ± 9	726 ± 9

[a] Data from the ref. 16.

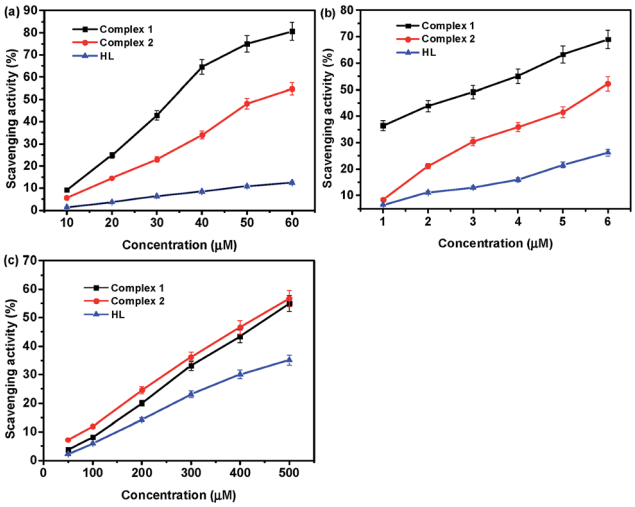

Fig. 9 Trends in the inhibition of DPPH, OH and NO radicals by complexes at various concentrations.

Cytotoxic activities

In vitro cytotoxic activities of the two complexes and cisplatin against two cancer cell lines human hepatocellular carcinoma cell line SMMC-7721 and human lung adenocarcinoma cell line A549 were conducted using a SRB assay in our study. The results were presented by means of cell viability curves and expressed as values in the studied concentration range from 0.1 to 100 μM. It is noteworthy that the IC_{50} values of complex **1** for the SMMC-7721 and A549 cell lines are 46.7 ± 1.2 and 39.5 ± 1.0 μM, and those of complex **2** are 66.6 ± 1.4 and 58.9 ± 1.2 μM, respectively. It is to be noted that the precursor and ligand did not display any inhibition of cell growth, even at concentrations of up to 100 mM, which clearly indicates that chelation of the ligand with the metal ion is responsible for the observed

cytotoxic properties of the complexes. The results of SRB assays revealed that the complexes exhibited notable activity against both SMMC-7721 and A549 cell lines. The cytotoxic activity of Ni(II) complex was found to be better when compared with the Co(II) complex, which may be attributed to the extended planar structure induced by the $\pi \rightarrow \pi$ conjugation resulting from the chelating of the Ni(II) with aroylhydrazone primary ligand and phen diimine co-ligand and the cationic nature of the complex.[17,39,72] Although the abovementioned complexes were active against the cell lines *in vitro* cytotoxicity experiments, none of the complexes could attain the effectiveness shown by the standard drug *cis*-platin (IC_{50} values of 18.0 and 25.3 μM, respectively).[66] The order of their *in vitro* anticancer activities is in agreement with their DNA-binding abilities, which supports the conclusion that DNA may be the primarily molecular target of these complexes. The IC_{50} values are much higher than those previously reported for other nickel complex containing a coordinated hydrazone with planar napthyl group, which is responsible for the selectivity and the potential inhibition against the tumour cells.[17] These findings suggest a strategy that increases the synergistic planarity and the cationic nature in mononuclear systems for the development of transition metal-based chemotherapeutic agents.

Conclusions

Two new Ni(II) and Co(II) complexes containing 2-acetonaphthone benzoyl hydrazone (HL) and 1,10-phenanthroline have been successfully synthesized and characterized by various spectral and analytical techniques. The molecular structure of the complexes was confirmed by single crystal X-ray diffraction studies. The DNA-binding interaction of the compounds has been evaluated by UV-vis and fluorescence spectroscopy which revealed that both complexes can bind to DNA *via* intercalation in the order of HL < Co(II) complex < Ni(II) complex. Binding affinity of the compounds with BSA was significant and the synchronous spectral studies showed that the complexes bound with BSA in both tyrosine and tryptophan residues. From the above results we observed that Ni(II) complex exhibited higher DNA and BSA binding affinity that Co(II) complex, which could be ascribed to the smaller size of Ni(II) complex to fit well into the DNA/BSA grooves than the bulkier cation of Co(II) complex. Also, the antioxidant and cytotoxicity properties of the newly synthesised complexes showed that they can be investigated in detail as potential drugs. In addition, both complexes exhibited significant cytotoxicity against SMMC-7721 and A549 cell lines. The present study highlighted that synergistic planarity of aroylhydrazone primary ligand and diimine co-ligand, as well as the cationic nature of the complex may play an important role in biological activities, suggesting that the DNA/BSA-binding activities as well as the cytotoxicity can be tuned by changing the ligands and the geometry in these nickel and cobalt systems. This is a step toward enabling the rational design of novel metallodrugs.

Conflicts of interest

There are no conflicts to declare.

Acknowledgements

The authors gratefully thanked the facilities support from Jiangsu Key Lab for the Chemistry & Utilization of Agricultural and Forest Biomass and supported by the Natural Science Foundation of Hainan Province (Grant No. 214035).

References

1 E. Wong and C. M. Giandomenico, *Chem. Rev.*, 1999, **99**, 2451–2466.
2 R. A. Alderden, M. D. Hall and T. W. Hambley, *J. Chem. Educ.*, 2006, **83**, 728.
3 E. R. Jamieson and S. J. Lippard, *Chem. Rev.*, 1999, **99**, 2467–2498.
4 W. Liu and R. Gust, *Chem. Soc. Rev.*, 2013, **42**, 755–773.
5 C. R. Munteanu and K. Suntharalingam, *Dalton Trans.*, 2015, **44**, 13796–13808.
6 S. H. van Rijt and P. J. Sadler, *Drug Discovery Today*, 2009, **14**, 1089–1097.
7 A. Bergamo and G. Sava, *Dalton Trans.*, 2011, **40**, 7817–7823.
8 C. Chitambar, *Future Med. Chem.*, 2012, **4**, 1257–1272.
9 I. Ott, *Coord. Chem. Rev.*, 2009, **253**, 1670–1681.
10 A. Bergamo, C. Gaiddon, J. H. M. Schellens, J. H. Beijnen and G. Sava, *J. Inorg. Biochem.*, 2012, **106**, 90–99.
11 G. Gasser, I. Ott and N. Metzler-Nolte, *J. Med. Chem.*, 2011, **54**, 3–25.
12 M. C. Heffern, N. Yamamoto, R. J. Holbrook, A. L. Eckermann and T. J. Meade, *Curr. Opin. Chem. Biol.*, 2013, **17**, 189–196.
13 G. Barone, A. Terenzi, A. Lauria, A. M. Almerico, J. M. Leal, N. Busto and B. García, *Coord. Chem. Rev.*, 2013, **257**, 2848–2862.
14 M. D. Hall, T. W. Failes, N. Yamamoto and T. W. Hambley, *Dalton Trans.*, 2007, 3983–3990.
15 R. Raj Kumar and R. Ramesh, *RSC Adv.*, 2015, **5**, 101932–101948.
16 D. S. Raja, N. S. P. Bhuvanesh and K. Natarajan, *Dalton Trans.*, 2012, **41**, 4365–4377.
17 P. Sathyadevi, P. Krishnamoorthy, R. R. Butorac, A. H. Cowley, N. S. P. Bhuvanesh and N. Dharmaraj, *Dalton Trans.*, 2011, **40**, 9690–9702.
18 P. Krishnamoorthy, P. Sathyadevi, A. H. Cowley, R. R. Butorac and N. Dharmaraj, *Eur. J. Med. Chem.*, 2011, **46**, 3376–3387.
19 M. P. Sathisha, U. N. Shetti, V. K. Revankar and K. S. R. Pai, *Eur. J. Med. Chem.*, 2008, **43**, 2338–2346.
20 P. Krishnamoorthy, P. Sathyadevi, R. R. Butorac, A. H. Cowley, N. S. P. Bhuvanesh and N. Dharmaraj, *Dalton Trans.*, 2012, **41**, 6842–6854.
21 N. R. Filipovic, S. Bjelogrlic, T. R. Todorovic, V. A. Blagojevic, C. D. Muller, A. Marinkovic, M. Vujcic, B. Janovic, A. S. Malesevic, N. Begovic, M. Sencanski and D. M. Minic, *RSC Adv.*, 2016, **6**, 108726–108740.
22 S. Tsiliou, L.-A. Kefala, F. Perdih, I. Turel, D. P. Kessissoglou and G. Psomas, *Eur. J. Med. Chem.*, 2012, **48**, 132–142.

23 F. Dimiza, A. N. Papadopoulos, V. Tangoulis, V. Psycharis, C. P. Raptopoulou, D. P. Kessissoglou and G. Psomas, *J. Inorg. Biochem.*, 2012, **107**, 54–64.
24 J. Haribabu, K. Jeyalakshmi, Y. Arun, N. S. P. Bhuvanesh, P. T. Perumal and R. Karvembu, *RSC Adv.*, 2015, **5**, 46031–46049.
25 P. Krishnamoorthy, P. Sathyadevi, P. T. Muthiah and N. Dharmaraj, *RSC Adv.*, 2012, **2**, 12190–12203.
26 T. W. Hambley, *Dalton Trans.*, 2007, 4929–4937.
27 M. V. Angelusiu, S.-F. Barbuceanu, C. Draghici and G. L. Almajan, *Eur. J. Med. Chem.*, 2010, **45**, 2055–2062.
28 V. P. Singh, S. Singh, D. P. Singh, P. Singh, K. Tiwari, M. Mishra and R. J. Butcher, *Polyhedron*, 2013, **56**, 71–81.
29 S. Mondal, B. Pakhira, A. J. Blake, M. G. B. Drew and S. K. Chattopadhyay, *Polyhedron*, 2016, **117**, 327–337.
30 S. Ramakrishnan, V. Rajendiran, M. Palaniandavar, V. S. Periasamy, B. S. Srinag, H. Krishnamurthy and M. A. Akbarsha, *Inorg. Chem.*, 2009, **48**, 1309–1322.
31 A. N. Wein, A. T. Stockhausen, K. I. Hardcastle, M. R. Saadein, S. Peng, D. Wang, D. M. Shin, Z. Chen and J. F. Eichler, *J. Inorg. Biochem.*, 2011, **105**, 663–668.
32 S. Anbu, R. Ravishankaran, A. A. Karande and M. Kandaswamy, *Dalton Trans.*, 2012, **41**, 12970–12983.
33 A. Basu, D. Thiyagarajan, C. Kar, A. Ramesh and G. Das, *RSC Adv.*, 2013, **3**, 14088–14098.
34 A. Erdem and M. Ozsoz, *Electroanalysis*, 2002, **14**, 965–974.
35 H. Xu, K.-C. Zheng, Y. Chen, Y.-Z. Li, L.-J. Lin, H. Li, P.-X. Zhang and L.-N. Ji, *Dalton Trans.*, 2003, 2260–2268.
36 M. Asadi, E. Safaei, B. Ranjbar and L. Hasani, *New J. Chem.*, 2004, **28**, 1227–1234.
37 E. Ramachandran, D. S. Raja, J. L. Mike, T. R. Wagner, M. Zeller and K. Natarajan, *RSC Adv.*, 2012, **2**, 8515–8525.
38 S. Ramakrishnan, E. Suresh, A. Riyasdeen, M. A. Akbarsha and M. Palaniandavar, *Dalton Trans.*, 2011, **40**, 3245–3256.
39 G. Ayyannan, M. Mohanraj, G. Raja, N. Bhuvanesh, R. Nandhakumar and C. Jayabalakrishnan, *Inorg. Chim. Acta*, 2016, **453**, 562–573.
40 Y. Li, Z. Yang, B. Song, H. Xia and Z. Wang, *Inorg. Nano-Met. Chem.*, 2017, **47**, 966–972.
41 *Bruker SMART and SAINT*, Bruker AXS Inc., Madison, Wisconsin, USA, 2002.
42 G. M. Sheldrick, SADABS, *Program for Empirical Absorption Correction of Area Detector*, University of Gottingen, Germany, 1996.
43 G. M. Sheldrick, *Acta Crystallogr., Sect. A: Found. Crystallogr.*, 2008, **64**, 112–122.
44 M. E. Reichmann, S. A. Rice, C. A. Thomas and P. Doty, *J. Am. Chem. Soc.*, 1954, **76**, 3047–3053.
45 G. Felsenfeld and S. Z. Hirschman, *J. Mol. Biol.*, 1965, **13**, 407–427.
46 S. Satyanarayana, J. C. Dabrowiak and J. B. Chaires, *Biochemistry*, 1992, **31**, 9319–9324.
47 M. S. Blois, *Nature*, 1958, **181**, 1199–1200.
48 C. C. Winterbourn, *Biochem. J.*, 1981, **198**, 125–131.
49 L. C. Green, D. A. Wagner, J. Glogowski, P. L. Skipper, J. S. Wishnok and S. R. Tannenbaum, *Anal. Biochem.*, 1982, **126**, 131–138.
50 L.-H. Jia, R.-Y. Li, Z.-M. Duan, S.-D. Jiang, B.-W. Wang, Z.-M. Wang and S. Gao, *Inorg. Chem.*, 2011, **50**, 144–154.
51 P. Sathyadevi, P. Krishnamoorthy, R. R. Butorac, A. H. Cowley and N. Dharmaraj, *Metallomics*, 2012, **4**, 498–511.
52 S. Naskar, S. Naskar, R. J. Butcher and S. K. Chattopadhyay, *Inorg. Chim. Acta*, 2010, **363**, 3641–3646.
53 M. S. Kryatova, O. V. Makhlynets, A. Y. Nazarenko and E. V. Rybak-Akimova, *Inorg. Chim. Acta*, 2012, **387**, 74–80.
54 E. C. Long and J. K. Barton, *Acc. Chem. Res.*, 1990, **23**, 271–273.
55 M. Alagesan, N. S. P. Bhuvanesh and N. Dharmaraj, *Dalton Trans.*, 2013, **42**, 7210–7223.
56 M. Sirajuddin, S. Ali and A. Badshah, *J. Photochem. Photobiol., B*, 2013, **124**, 1–19.
57 A. Wolfe, G. H. Shimer and T. Meehan, *Biochemistry*, 1987, **26**, 6392–6396.
58 B.-d. Wang, Z.-Y. Yang, Q. Wang, T.-k. Cai and P. Crewdson, *Bioorg. Med. Chem.*, 2006, **14**, 1880–1888.
59 J. Ravichandran, P. Gurumoorthy, M. A. Imran Musthafa and A. Kalilur Rahiman, *Spectrochim. Acta, Part A*, 2014, **133**, 785–793.
60 P. A. Vekariya, P. S. Karia, J. V. Vaghasiya, S. Soni, E. Suresh and M. N. Patel, *Polyhedron*, 2016, **110**, 73–84.
61 Y.-J. Hu, Y. Liu, J.-B. Wang, X.-H. Xiao and S.-S. Qu, *J. Pharm. Biomed. Anal.*, 2004, **36**, 915–919.
62 P. Sathyadevi, P. Krishnamoorthy, E. Jayanthi, R. R. Butorac, A. H. Cowley and N. Dharmaraj, *Inorg. Chim. Acta*, 2012, **384**, 83–96.
63 K. Karami, Z. Mehri Lighvan, A. M. Alizadeh, M. Poshteh-Shirani, T. Khayamian and J. Lipkowski, *RSC Adv.*, 2016, **6**, 78424–78435.
64 A. S. Sharma, S. Anandakumar and M. Ilanchelian, *RSC Adv.*, 2014, **4**, 36267–36281.
65 F. Samari, B. Hemmateenejad, M. Shamsipur, M. Rashidi and H. Samouei, *Inorg. Chem.*, 2012, **51**, 3454–3464.
66 X.-W. Li, X.-J. Li, Y.-T. Li, Z.-Y. Wu and C.-W. Yan, *J. Photochem. Photobiol., B*, 2013, **118**, 22–32.
67 D. Senthil Raja, N. S. P. Bhuvanesh and K. Natarajan, *Inorg. Chem.*, 2011, **50**, 12852–12866.
68 X.-Z. Feng, Z. Lin, L.-J. Yang, C. Wang and C.-l. Bai, *Talanta*, 1998, **47**, 1223–1229.
69 E. U. Akusoba and J. N. Miller, *Proc. Anal. Div. Chem. Soc.*, 1979, **16**, 92–95.
70 J. Tang, F. Luan and X. Chen, *Bioorg. Med. Chem.*, 2006, **14**, 3210–3217.
71 L. Tabrizi, P. McArdle, A. Erxleben and H. Chiniforoshan, *Eur. J. Med. Chem.*, 2015, **103**, 516–529.
72 F. A. Beckford, J. M. Shaloski, G. Leblanc, J. Thessing, L. C. Lewis-Alleyne, A. A. Holder, L. Li and N. P. Seeram, *Dalton Trans.*, 2009, 10757–10764.